

VanQver: The Variational and Adiabatically Navigated Quantum Eigensolver

Shunji Matsuura, Takeshi Yamazaki, Valentin Senicourt, and Arman Zaribafiyani
1QB Information Technologies (1QBit), Vancouver, British Columbia, V6C 2B5, Canada

(Dated: September 4, 2022)

The accelerated progress in manufacturing noisy intermediate-scale quantum (NISQ) computing hardware has opened the possibility of exploring its application in transforming approaches to solving computationally challenging problems. The important limitations common among all NISQ computing technologies are the absence of error correction and the short coherence time, which limit the computational power of these systems. Shortening the required time of a single run of a quantum algorithm is essential for reducing environment-induced errors and for the efficiency of the computation. We have investigated the ability of a variational version of adiabatic quantum computation (AQC) to generate an accurate state more efficiently compared to existing adiabatic methods. The standard AQC method uses a time-dependent Hamiltonian, connecting the initial Hamiltonian with the final Hamiltonian. In the current approach, a navigator Hamiltonian is introduced which has a finite amplitude only in the middle of the annealing process. Both the initial and navigator Hamiltonians are determined using variational methods. The cluster operator of coupled-cluster theory, truncated to single and double excitations, is used as a navigator Hamiltonian. A comparative study of our variational algorithm (VanQver) with that of standard AQC, starting with a Hartree–Fock Hamiltonian, is presented. The results indicate that the introduction of the navigator Hamiltonian significantly improves the annealing time required to achieve chemical accuracy by two to three orders of magnitude. The efficiency of the method is demonstrated in the ground-state energy estimation of molecular systems, namely, H_2 , P_4 , and LiH .

I. INTRODUCTION

Due to the inherent many-body nature of quantum systems, obtaining energetically stable quantum states is one of the most difficult problems in computational chemistry and physics. Despite decades of advancements in classical hardware and algorithms for simulating quantum systems, many important problems, such as computing electronic correlation energies and predicting chemical reaction rates, remain largely unsolved. In order to obtain accurate results, highly precise numerical methods are required, such as full configuration interaction (FCI) and coupled-cluster theory. The computational resources required to run these precise methods grows with the system size to the extent that even state-of-art supercomputers can handle only small-sized problems [1]. Researchers have attempted to alleviate this issue by introducing heuristics and approximation techniques like problem decomposition methods to reduce the computational complexity of this problem. This establishes a trade-off between the accuracy of the approximate solution and the computational efficiency. In addition, a lot of effort has been put towards the exploration of other paradigms of computation. Quantum computing, for example, is a promising approach to mitigating this problem [2, 3]. There has been a recent increase in the number of experiments in simulating quantum systems on quantum devices [4–13]. The difficulty faced in these experiments is in executing operations without losing relevant quantum coherence. Whereas quantum error correction will make it possible to perform an unlimited number of operations, the required resources are very great, well beyond the capabilities of current hardware. Therefore, the development of methods that require less-stringent

quantum coherence is essential for near-term quantum devices. A subset of the authors of the present work have previously investigated the idea of combining problem decomposition techniques in conjunction with quantum computing approaches [14]. Quantum–classical hybrid algorithms, such as the variational quantum eigensolver (VQE) [15–17], are suitable from this perspective. In addition to the algorithm requiring a shorter coherence time, the VQE has demonstrated robustness against systematic control errors [8–10].

Thus far, most of the experiments that have made use of the VQE and phase estimation algorithms (PEA) [18, 19] have been performed within the framework of gate model quantum computation. An alternative framework is adiabatic quantum computation (AQC) [20–26]. AQC solves computational problems by continuously evolving a Hamiltonian. As such, it is absent of algorithmic errors (e.g. Trotterization errors). It is also robust against certain types of decoherence [27–31]. Whereas gate model quantum computation is not meaningfully executed beyond the qubit dephasing time [32], the annealing time T in AQC can be longer than the qubit coherence time under certain conditions. For instance, when the interaction between the quantum system and environment is weak, the decoherence occurs in the energy eigenbasis of the system. In this case, the coherence of the instantaneous ground state, relevant for AQC, is preserved [27]. Nevertheless, the long annealing time in open quantum systems can cause problems. For instance, it induces thermalization and the probability of finding a ground state decays exponentially at a fixed temperature as the problem size increases [33]. Therefore, effort towards shortening the annealing time is essential and critical for the success of AQC. The com-

putational time in AQC is constrained by various factors. From the perspective of computational efficiency and the prevention of bath-induced errors, a shorter annealing time is desirable, whereas, in order to avoid errors due to non-adiabatic transitions, the computational time needs to be longer than the scale of the inverse energy gap between the ground state and excited states during the annealing process. In this work, we investigate a variational AQC method and demonstrate that it can significantly reduce annealing time.

II. THE VARIATIONAL AND ADIABATICALLY NAVIGATED QUANTUM EIGENSOLVER

In the standard form of AQC, the time-dependent Hamiltonian is given by

$$H(t) = A(t)H_{\text{ini}} + B(t)H_{\text{fin}}, \quad (1)$$

where the functions $A(t)$ and $B(t)$ satisfy the conditions that $A(0) \gg B(0) = 0$ and $B(T) \gg A(T) = 0$, respectively. Here, T is the annealing time and $t \in [0, T]$. Hereafter, we use the phrase ‘‘standard AQC’’ for (1) with the boundary conditions for $A(t)$ and $B(t)$.

In the variational approach, we introduce a navigator Hamiltonian that has a non-zero amplitude only during the annealing process. This navigator Hamiltonian, $H_{\text{nav}}(\boldsymbol{\theta})$, is characterized by variational parameters $\boldsymbol{\theta}$. Adding an extra term to the Hamiltonian has previously been considered (see Refs. [17, 34–36]). We take advantage of the fact that the initial Hamiltonian H_{ini} is not uniquely determined, and treat its parameters as variational: $H_{\text{ini}}(\boldsymbol{\eta})$. The variational parameters $\boldsymbol{\eta}$ may need to satisfy certain constraints. We will address this aspect with concrete molecular models in Sec. III. Note that even though different values of $\boldsymbol{\eta}$ may have the same initial ground state, they generate different quantum states during annealing. A motivation for introducing $H_{\text{ini}}(\boldsymbol{\eta})$ and $H_{\text{nav}}(\boldsymbol{\theta})$ with variational parameters is that the efficiency of AQC can be highly dependent on the annealing paths. The problem is that we do not *a priori* know what kinds of terms would be beneficial for specific problems. The variational parameters in AQC navigate the quantum state along the path that provides a higher probability of finding the true ground state, even when the annealing time is shorter than expected from standard AQC (1). We call this algorithm the ‘‘Variational and Adiabatically Navigated Quantum Eigensolver’’ (VanQver). The time-dependent Hamiltonian in VanQver is

$$H_{(\boldsymbol{\eta}, \boldsymbol{\theta})}(t) = A(t)H_{\text{ini}}(\boldsymbol{\eta}) + B(t)H_{\text{fin}} + C(t)H_{\text{nav}}(\boldsymbol{\theta}). \quad (2)$$

The coefficient $C(t)$ satisfies the boundary conditions $C(0) = C(T) = 0$, while its value is non-zero during annealing, $0 < t < T$. A natural choice of the boundary conditions for A and B will be the same as that in standard AQC. There can be multiple initial and navigator Hamiltonians, each with a different time-dependence

value. At the end of the annealing process, the quantum device generates a certain state. We measure the expectation value of the final Hamiltonian H_{fin} . If H_{fin} is a quantum Hamiltonian, single-qubit rotations may be needed prior to performing measurements. We send the data of the expectation value $E = \langle H_{\text{fin}} \rangle$ and the variational parameters $\boldsymbol{\theta}$ and $\boldsymbol{\eta}$ to a classical computer, where a classical optimizer will return a new set of variational parameters. With the new set of parameters, we run AQC on the quantum device and then measure the energy. We repeat this cycle until the energy converges. The process is summarized in Fig. 1. More-detailed steps of this algorithm are provided in Appendix B.

In this work, we focus on investigating VanQver in the context of quantum chemistry simulation. However, the use of the algorithm itself can be much more general. For instance, in solving combinatorial optimization problems, one could view VanQver as a refinement and a unification of previously studied techniques, such as the use of an anti-ferromagnetic driver Hamiltonian (i.e., a nonstoquastic Hamiltonian) [36–41], the use of an inhomogeneous driver Hamiltonian [42–44], and reverse annealing [35, 45]. Reverse annealing is a method for annealing backwards from a particular state by increasing quantum fluctuations and then reducing them in order to reach a new state. It has been implemented on D-Wave Systems’ quantum annealer [45, 46]. In [35], a uniform transverse field is considered as an additional Hamiltonian with a ‘‘sombbrero-like’’ time-dependent amplitude (similar to H_{nav} in VanQver, but with different functionality), while the initial Hamiltonian is diagonal in the computational basis and updated iteratively with heuristic guesses. Whereas these specific methods can improve computational results in certain cases, guidelines for applying them to general models are needed. Unlike in the works cited above, VanQver keeps a variational transverse field as the driver Hamiltonian while adding a prominence-like navigator Hamiltonian. This algorithm constitutes a blueprint for one approach to solving this problem.

III. MOLECULAR SYSTEMS

Let us consider the problem of obtaining the ground state energy of a molecule. Under Born–Oppenheimer approximation, the second quantized form of molecular electronic Hamiltonian is read as

$$H_{\text{fin}}^{\text{ferm}} = \sum_{pq} h_{pq} a_p^\dagger a_q + \frac{1}{2} \sum_{pqrs} h_{pqrs} a_p^\dagger a_q^\dagger a_r a_s, \quad (3)$$

where p, q, r , and s label spin-orbitals and a_p^\dagger and a_p are creation and annihilation operators of an electron in spin-orbital p , while h_{pq} and h_{pqrs} are one- and two-electron integrals. Under Bravyi–Kitaev (BK) or Jordan–Wigner (JW) transformations, Eq. (3) is translated into a qubit Hamiltonian $H_{\text{fin}}^{\text{qubit}}$. A natural ini-

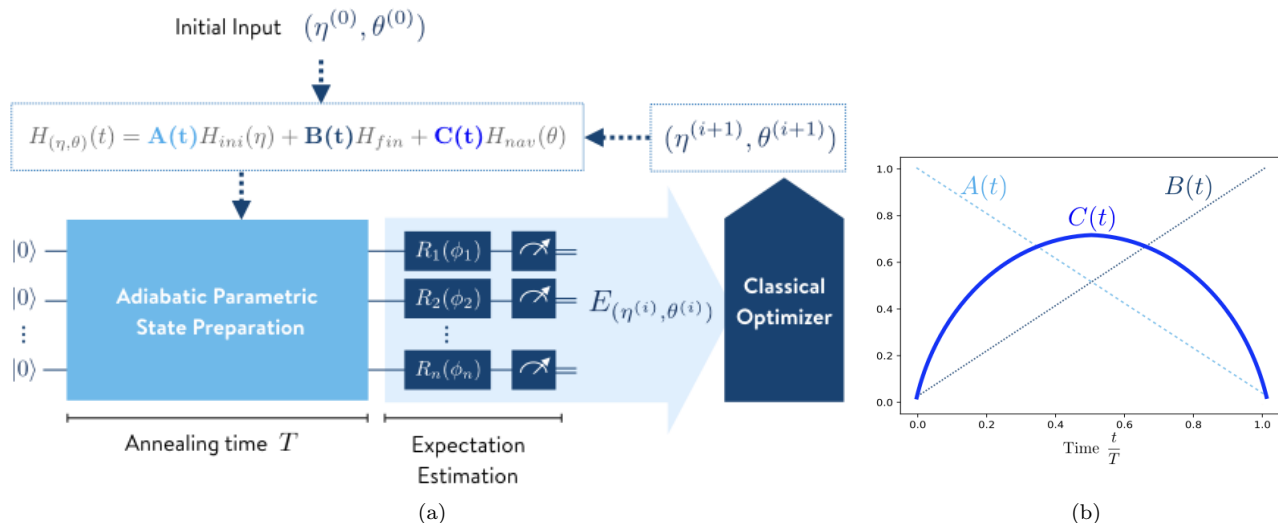


FIG. 1. (a) A schematic illustration of the quantum–classical hybrid VanQver algorithm, and (b) a schematic illustration of the time dependent amplitudes of H_{ini} , H_{nav} , and H_{fin} .

tial Hamiltonian consists of one-electron terms, which include the Hartree–Fock (HF) Hamiltonian. For simplicity, we use a 1-local qubit Hamiltonian in the rest of our experiments:

$$H_{ini}^{\text{qubit}} = \sum_p \eta_p \sigma_p^z. \quad (4)$$

While the η_p take specific values in the HF Hamiltonian, we treat them as variational parameters in VanQver. However, there is an important symmetry constraint. The signs of η_p determine which spin-orbitals are occupied or virtual. Since the electron number operator N and spin number operators $N_{\uparrow, \downarrow}$, or a parity of them, commute with H_{ini} , H_{fin} , and cluster operators (H_{nav}), these numbers are constant during annealing. Therefore, the signs of η_p directly determine the state of the molecule, such as being neutral or ionic, at the end of the annealing process. We vary the parameters η_p while keeping their signs.

The choice of the navigator Hamiltonian is important for the efficiency of VanQver. Inspired by the promising results of VQE using unitary coupled-cluster (UCC) ansatz, we propose to use a cluster operator as the navigator Hamiltonian in our molecular simulations.

The cluster operator truncated to single and double excitations is

$$H_{nav}^{\text{ferm}} = \sum_{\substack{i \in \text{occ} \\ \alpha \in \text{vir}}} \theta_{i\alpha} a_i^\dagger a_\alpha + \sum_{\substack{ij \in \text{occ} \\ \alpha\beta \in \text{vir}}} \theta_{ij\alpha\beta} a_i^\dagger a_j^\dagger a_\alpha a_\beta + h.c., \quad (5)$$

where $h.c.$ is the Hermitian conjugate. One can add higher-order excitation terms as well. In VQE, the entire quantum operation is a realization of the Trotterized exponential of an anti-Hermitian cluster operator, and the accuracy of the obtained energy is limited by which excitations are included. For instance, an exact state

can be obtained if all possible excitation operators are included, whereas the use of only single excitation operators with the HF initial state may not significantly improve the performance due to Brillouin’s theorem, which states that the HF ground state cannot be improved by mixing it with singly excited determinants. In VanQver, a quantum state can, in principle, reach the exact state without the cluster operator. Therefore, the accuracy is not limited by the type of excitation operators in H_{nav} . The role of a cluster operator is to *assist* in reaching the exact state as closely as possible within a shorter annealing time T .

IV. NUMERICAL RESULTS

The performance of VanQver was tested by solving the time-dependent Schrödinger equation directly on classical hardware. The calculations were performed using the library QuTip [47, 48]. The annealing schedule used was $A(t) = 1 - (\frac{t}{T})^2$, $B(t) = (\frac{t}{T})^2$ and $C(t) = \alpha \frac{t}{T} (1 - \frac{t}{T})$, where α is a numerical constant which can be renormalized to 1 by rescaling θ . The initial parameters $\theta^{(0)}$ were set to zero and $\eta^{(0)} = \text{sign}(\eta_{\text{HF}})$, where η_{HF} are the coefficients in the HF Hamiltonian. All the parameters were updated using an optimizer on a classical computer. The test set included H_2 , P4 (two hydrogen molecules parallel to each other) for various values of the separation distance d , and LiH. The graphical picture of the molecules is in Appendix A. The nuclear separation distances for both H_2 and LiH were chosen to be 1 Å. For P4, the nuclear separation distance for each of the hydrogen molecules was 2 Å, and the separation distance d between the two hydrogen molecules varied from $d = 0.4$ Å

to $d = 4.0$ Å. In what follows, units of distance are always expressed in ångströms. Also note that a minimal basis set (STO-3G) is employed in all calculations. In this case, H₂, P4, and LiH were described using 4, 8, and 12 qubits, respectively. Note that the number of qubits can be reduced based on \mathbb{Z}_2 symmetries [9, 49].

The Broyden–Fletcher–Goldfarb–Shanno (BFGS) algorithm was used as a classical optimizer and the tolerance for termination (ϵ_{tol}) was set to $\epsilon_{\text{tol}} = 0.001, 0.0005,$ and 0.0001 . The converged parameters ($\boldsymbol{\eta}^{\text{final}}, \boldsymbol{\theta}^{\text{final}}$) provided the annealing path, which brought the quantum state closest to the exact ground state in a given annealing time T .

Note that T is the annealing time of a *single* run. The total computational time needs to take into account the repeated runs of the quantum device as well as the computational overhead for the classical optimizer. However, the limitation of near-term quantum hardware is the coherence time of a single run. Therefore, the main focus was on the relation between the annealing time T and the expectation value of the energy E obtained using $\boldsymbol{\eta}^{\text{final}}$ and $\boldsymbol{\theta}^{\text{final}}$.

We compared the performance of VanQver with the standard AQC (1). The initial Hamiltonian was chosen to be a canonical RHF Hamiltonian, as considered in Ref. [50],

$$H_{\text{MP}} = \sum_p f_{pp} a_p^\dagger a_p, \\ f_{pp} = h_{pp} + \sum_{i \in \text{occ}} (\langle pi|pi \rangle - \langle pi|ip \rangle), \quad (6)$$

where h_{pp} are the one-electron integrals and $\langle pi|pi \rangle$ and $\langle pi|ip \rangle$ are direct (Coulomb) and exchange two-electron integrals. Here, MP refers to Møller–Plesset, since this is the unperturbed form of the Hamiltonian used in MP perturbation theory. These terms of the Hamiltonian sum up to become the Fock operator.

Fig. 2 shows the obtained energy E with ($\boldsymbol{\eta}^{\text{final}}, \boldsymbol{\theta}^{\text{final}}$) as a function of the annealing time T for the P4 molecule with separation distance $d = 0.8$ and termination tolerance $\epsilon_{\text{tol}} = 0.001$. The energy is expressed in hartrees and the unit of the annealing time depends on the realization of the Hamiltonian on quantum hardware. The time evolution used in the numerical simulation is $\mathcal{T} \exp(-i \int_0^T H dt)$, where \mathcal{T} is the time ordering. Results for H₂ and LiH are shown in Appendix C. The red points represent the results obtained with VanQver, while the green lines represent the results obtained with standard adiabatic evolution (1) when H_{MP} (6) was used for H_{ini} . The horizontal dotted line in blue corresponds to the exact energies, the horizontal dotted line in magenta shows the error from the exact energies within chemical accuracy (1.0 kcal/mol), and the horizontal dotted line in black represents the Hartree–Fock energy. The inset shows the very short annealing time region. This result shows that VanQver allows us to reach chemical accuracy within a much shorter time compared to the

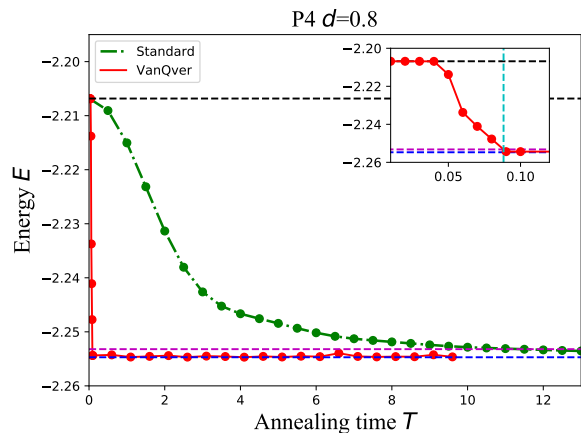


FIG. 2. Energy of P4 with $d = 0.8$ as a function of annealing time T . The inset shows the region $0 \leq T \leq 0.12$. The red points represent the results obtained using VanQver, the green points represent the results obtained with standard AQC with $H_{\text{ini}} = H_{\text{MP}}$, and the dotted lines in blue and magenta dotted lines represent the exact and chemical accuracy energies, respectively. $T_{CA}^{\text{VanQver}} = 0.088$ for VanQver, whereas $T_{CA}^{\text{Standard}} = 11.5$ without using VanQver.

standard AQC time evolution (1). The annealing time to reach chemical accuracy, T_{CA} , is $T_{CA}^{\text{VanQver}} = 0.088$ for VanQver, whereas $T_{CA}^{\text{Standard}} = 11.5$ when VanQver is not used. We emphasize that $T_{CA}^{\text{VanQver/Standard}}$ is defined as the annealing time for a single run. Another interesting point is that when the annealing time was too short, the energy stayed at the HF energy, and that the quantum states did not evolve very much from the initial state. Therefore, the final state was still close to the reference state. Once the annealing time became longer, the effect of the H_{nav} was very strong and the energy dropped rapidly. Note that while the change of $\boldsymbol{\eta}$ within the appropriate parameter region did not change the initial state, it did change the evolution during the annealing process. Therefore, we changed $\boldsymbol{\eta}$ depending on the values of $\boldsymbol{\theta}$.

Fig. 3 shows the results for P4 with $d = 2.0$. In this case, the result shows slightly different features. Similar to the case of P4 with $d = 0.8$, the energy stayed at the HF energy when the annealing time was too short, and then dropped rapidly. In the case of $d = 2.0$, the energy did not reach chemical accuracy immediately. Instead, it decreased gradually after the rapid drop and then eventually reached chemical accuracy at $T_{CA}^{\text{VanQver}} = 9.855$. The annealing time required to reach chemical accuracy was much longer than when $d = 0.8$. However, the required time using standard AQC was much longer: $T_{CA}^{\text{Standard}} = 456$. Therefore, once again, $T_{CA}^{\text{VanQver}} \ll T_{CA}^{\text{Standard}}$. We investigated how VanQver compared to a conventional CCSD calculation on this system. The energy as a function of the separation distance for CCSD and the exact results are shown in Fig. 4. As is well-known, in order

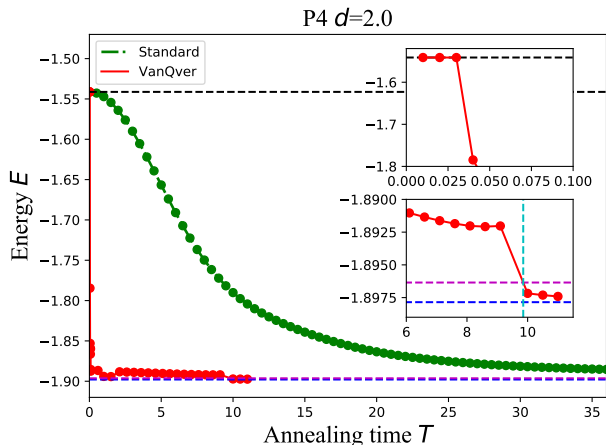


FIG. 3. Energy as a function of annealing time T for P4 with $d = 2.0$. The exact energy (FCI energy) is -1.8978 . The energy drops rapidly from $T = 0.03$ to $T = 0.1$. The annealing times to reach chemical accuracy are $T_{CA}^{\text{VanQver}} = 9.855327037$ for VanQver and $T_{CA}^{\text{Standard}} = 456$ for standard AQC. The plot shows only $T \leq 36$. The upper inset shows the time window in which the energy drops rapidly from the HF energy. The lower inset shows the time window in which the energy achieves chemical accuracy.

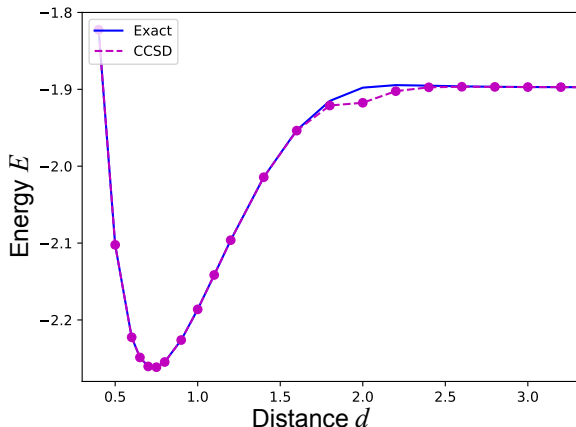


FIG. 4. Energy as a function of intermolecular separation distance for P4. The blue line represents the exact result, and the dotted line in magenta represents the CCSD results.

to obtain accurate results for the P4 system both at and around $d = 2.0$ (i.e., a square geometry), we would need to add the quadruple excitations (exact) or use a multi-reference correlation approach. This is due to the fact that two configurations become degenerate as d tends towards a value of 2.0, in this system. This is a well-known pathological multi-reference case demonstrating the failures of conventional single-reference methods like CCSD. This is also reflected in the longer annealing times of the AQC simulations, both with the standard method (using a canonical RHF Hamiltonian) and VanQver. We

emphasize that while CCSD failed in providing even a qualitative description of the potential energy surface at this geometry, in VanQver one can achieve chemical accuracy with the navigator Hamiltonian of Eq. (5) by taking annealing time $T \geq T_{CA}^{\text{VanQver}}$.

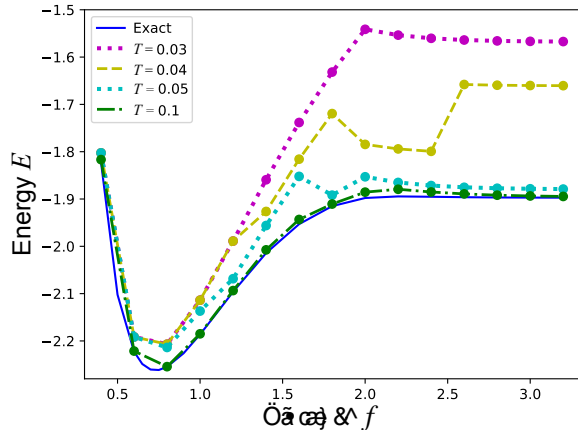


FIG. 5. Energy of P4 for various values of the intermolecular separation distance d at fixed annealing times $T = 0.03, 0.04, 0.05$, and 0.1 . The tolerance for the termination is 0.001 .

In Fig. 5, we show the energy as a function of the separation distance d for fixed annealing times T . The points in magenta, yellow, cyan, and green represent $T = 0.03, 0.04, 0.05$, and 0.1 . The blue line represents the exact energy (FCI energy). When the annealing time was too short ($T = 0.03$), VanQver did not improve the results and recovered the HF energies. As the annealing time was slightly increased to $T = 0.04, 0.05$, and 0.1 , the energies rapidly improved. The final energy for a given annealing time T depended on the tolerance of the termination. Even with short annealing times, the obtained energy was able to be much improved as the tolerance ϵ_{tol} changed from 0.001 to 0.0005 , in exchange for an increase in iterations. For instance, $E = -1.541$ for $T = 0.03$ with $\epsilon_{\text{tol}} = 0.001$, while $E = -1.848$ for $T = 0.03$ with $\epsilon_{\text{tol}} = 0.0005$, which was a significant improvement. On the other hand, we did not see a large difference between $\epsilon_{\text{tol}} = 0.0005$ and $\epsilon_{\text{tol}} = 0.0001$. The tolerance dependence of the energy and the number of iterations are shown in Fig. 10(a) and Fig. 10(b) in Appendix D.

Fig. 6 shows a comparison of the annealing time to chemical accuracy for VanQver and standard AQC for different distances of d in P4. A logarithmic scale is used for T_{CA} in the inset. The general features of the two results are similar. When the required annealing time is longer in standard AQC, similar behaviour is observed in VanQver. It is not surprising that the longest required annealing time is observed at an intermolecular separation of $d = 2.0$, since this is where the conventional CCSD method fails (Fig. 4), as discussed above. However, we would like to emphasize that the required annealing time

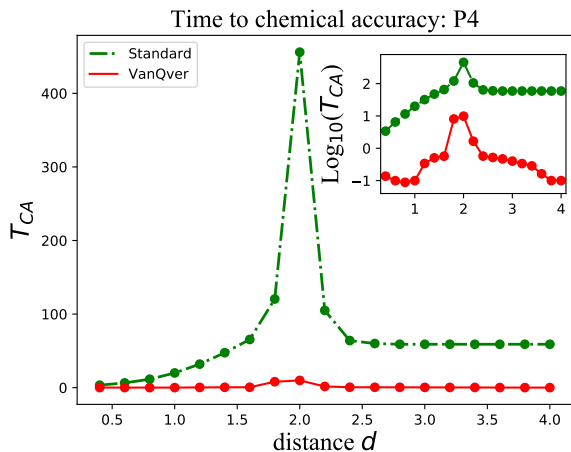


FIG. 6. The time to chemical accuracy T_{CA} for P4. The horizontal axis conveys the intermolecular separation distance d . The red points represent the VanQver results and the green points represent the standard AQC results with initial Hamiltonian H_{MP} . The time is in logarithmic scale, in the inset. It shows that T_{CA}^{VanQver} and T_{CA}^{Standard} differ by two to three orders of magnitude across the entire range of the intermolecular distance d .

is always one or two orders of magnitude shorter than that of standard AQC.

V. CONCLUSION

A hybrid algorithm VanQver was proposed and its efficiency was tested for the purpose of molecular energy estimation. The algorithm is essentially a variational quantum eigensolver that uses adiabatic evolution instead of a gate-based implementation of the state preparation. The adiabatic evolution, however, has been implemented using parametric Hamiltonians, which constitutes a parametric initial driver Hamiltonian, the final Hamiltonian describing the system under study and a parametric navigator Hamiltonian that increases the overlap of the final state with the desired outcome (in this case the state with the lowest eigenvalue). The amplitude of the navigator Hamiltonian is prominence-like, that is, it is gradually increased up to a point during the annealing process and then decreased such that at the end of adiabatic evolution the only Hamiltonian with a non-zero amplitude is the final Hamiltonian. As with the choice of ansatz in gate model VQE, the choice of parametric navigator Hamil-

tonian has a critical impact on the performance of this method. In the context of molecular energy estimation, we suggest using cluster operators introduced by unitary coupled-cluster theory.

As a measure of efficiency, the interdependence of annealing time and chemical accuracy were considered. The required annealing times for VanQver were found to be significantly lower than those of standard AQC. Although the shorter annealing time renders this algorithm more amenable to noisy near-term quantum hardware, it is yet to be determined if the shorter single-iteration runtime of variational algorithms also provides an advantage in terms of overall computational effort when scaling beyond near-term quantum computing technologies.

Additionally, when a quantum device is coupled to the environment, computational results are not monotonically improved as the annealing time increases. Therefore, it is important to analyze the performance of VanQver and standard AQC in the presence of noise. We look to address these issues in future work.

It should be noted that VanQver can also be used to solve optimization problems. In this case the final Hamiltonian will be diagonal in the computational basis and will therefore represent a classical energy function. Possible future work expanding on this research would be to determine the optimal choice of the navigator Hamiltonian to achieve shorter annealing time requirements for classical optimization problems. Ideas already exist in this respect, such as using a non-stoquastic Hamiltonian or an inhomogeneous transverse field. In some cases, taking non-adiabatic paths is much more efficient than taking adiabatic paths. Although it is difficult to determine which strategy to employ to shorten the time to solution, VanQver may be able to systematically survey various strategies.

VI. ACKNOWLEDGEMENT

The authors thank Marko Bucyk for reviewing and editing the manuscript. S. M. appreciates the hospitality of H. Nishimori and T. Takayanagi during his stay at the Tokyo Institute of Technology and the Yukawa Institute for Theoretical Physics. He also appreciates useful discussions with D. Lidar and P. Ronagh. We thank L. Huntington, Y. Kawashima, and P. Verma for valuable comments on a draft of the manuscript. We thank J. Loscher and A. Saidmuradov for technical support.

[1] M. Head-Gordon and E. Artacho, *Physics Today* **61**, 58 (2008).
 [2] R. Feynman, *International Journal of Theoretical Physics* **21**, 467 (1982).
 [3] S. Lloyd, *Science* **273**, 1073 (1996).

[4] A. Peruzzo, J. McClean, P. Shadbolt, M.-H. Yung, X.-Q. Zhou, P. J. Love, A. Aspuru-Guzik, and J. L. O’Brien, *Nature Communications* **5**, 4213 EP (2014).
 [5] J. Du, N. Xu, X. Peng, P. Wang, S. Wu, and D. Lu, *Phys. Rev. Lett.* **104**, 030502 (2010).

- [6] Y. Shen, X. Zhang, S. Zhang, J.-N. Zhang, M.-H. Yung, and K. Kim, *Phys. Rev. A* **95**, 020501 (2017).
- [7] Y. Wang, F. Dolde, J. Biamonte, R. Babbush, V. Bergholm, S. Yang, I. Jakobi, P. Neumann, A. Aspuru-Guzik, J. D. Whitfield, and J. Wrachtrup, *ACS Nano* **9**, 7769 (2015), pMID: 25905564, <https://doi.org/10.1021/acs.nano.5b01651>.
- [8] R. Santagati, J. Wang, A. A. Gentile, S. Paesani, N. Wiebe, J. R. McClean, S. Morley-Short, P. J. Shadbolt, D. Bonneau, J. W. Silverstone, D. P. Tew, X. Zhou, J. L. O'Brien, and M. G. Thompson, *Science Advances* **4** (2018), 10.1126/sciadv.aap9646.
- [9] P. J. J. O'Malley, R. Babbush, I. D. Kivlichan, J. Romero, J. R. McClean, R. Barends, J. Kelly, P. Roushan, A. Tranter, N. Ding, B. Campbell, Y. Chen, Z. Chen, B. Chiaro, A. Dunsworth, A. G. Fowler, E. Jeffrey, A. Megrant, J. Y. Mutus, C. Neill, C. Quintana, D. Sank, A. Vainsencher, J. Wenner, T. C. White, P. V. Coveney, P. J. Love, H. Neven, A. Aspuru-Guzik, and J. M. Martinis, (2015), 10.1103/PhysRevX.6.031007, arXiv:1512.06860.
- [10] A. Kandala, A. Mezzacapo, K. Temme, M. Takita, M. Brink, J. M. Chow, and J. M. Gambetta, (2017), 10.1038/nature23879, arXiv:1704.05018.
- [11] J. S. Otterbach, R. Manenti, N. Alidoust, A. Bestwick, M. Block, B. Bloom, S. Caldwell, N. Didier, E. S. Fried, S. Hong, P. Karalekas, C. B. Osborn, A. Papageorge, E. C. Peterson, G. Prawiroatmodjo, N. Rubin, C. A. Ryan, D. Scarabelli, M. Scheer, E. A. Sete, P. Sivarajah, R. S. Smith, A. Staley, N. Tezak, W. J. Zeng, A. Hudson, B. R. Johnson, M. Reagor, M. P. da Silva, and C. Rigetti, "Unsupervised machine learning on a hybrid quantum computer," (2017), arXiv:1712.05771.
- [12] C. Hempel, C. Maier, J. Romero, J. McClean, T. Monz, H. Shen, P. Jurcevic, B. Lanyon, P. Love, R. Babbush, A. Aspuru-Guzik, R. Blatt, and C. Roos, "Quantum chemistry calculations on a trapped-ion quantum simulator," (2018), arXiv:1803.10238.
- [13] A. D. King, J. Carrasquilla, I. Ozfidan, J. Raymond, E. Andriyash, A. Berkley, M. Reis, T. M. Lanting, R. Harris, G. Poulin-Lamarre, A. Y. Smirnov, C. Rich, F. Altomare, P. Bunyk, J. Whittaker, L. Swenson, E. Hoskinson, Y. Sato, M. Volkmann, E. Ladizinsky, M. Johnson, J. Hilton, and M. H. Amin, "Observation of topological phenomena in a programmable lattice of 1,800 qubits," (2018), arXiv:1803.02047.
- [14] T. Yamazaki, S. Matsuura, A. Narimani, A. Saidmuradov, and A. Zaribafiyani, "Towards the practical application of near-term quantum computers in quantum chemistry simulations: A problem decomposition approach," (2018), arXiv:1806.01305.
- [15] A. Peruzzo, J. McClean, P. Shadbolt, M.-H. Yung, X.-Q. Zhou, P. J. Love, A. Aspuru-Guzik, and J. L. O'Brien, *Nat. Commun.* **5**, 4213 EP (2014).
- [16] M. H. Yung, J. Casanova, A. Mezzacapo, J. McClean, L. Lamata, A. Aspuru-Guzik, and E. Solano, *Scientific Reports* **4**, 3589 EP (2014).
- [17] J. R. McClean, J. Romero, R. Babbush, and A. Aspuru-Guzik, *New Journal of Physics* **18**, 023023 (2016).
- [18] D. S. Abrams and S. Lloyd, *Phys. Rev. Lett.* **79**, 2586 (1997).
- [19] A. Aspuru-Guzik, A. D. Dutoi, P. J. Love, and M. Head-Gordon, *Science* **309**, 1704 (2005).
- [20] A. B. Fimmel, M. A. Gomez, C. Sebenik, C. Stenson, and J. D. Doll, *Chemical Physics Letters* **219**, 343 (1994).
- [21] T. Kadowaki and H. Nishimori, *Phys. Rev. E* **58**, 5355 (1998).
- [22] E. Farhi, J. Goldstone, S. Gutmann, J. Lapan, A. Lundgren, and D. Preda, *Science* **292**, 472 (2001).
- [23] J. Brooke, D. Bitko, T. F., Rosenbaum, and G. Aeppli, *Science* **284**, 779 (1999).
- [24] J. Brooke, T. F. Rosenbaum, and G. Aeppli, *Nature* **413**, 610 (2001).
- [25] G. E. Santoro, R. Martoňák, E. Tosatti, and R. Car, *Science* **295**, 2427 (2002).
- [26] A. Das and B. K. Chakrabarti, *Rev. Mod. Phys.* **80**, 1061 (2008).
- [27] T. Albash and D. A. Lidar, *Phys. Rev. A* **91**, 062320 (2015).
- [28] A. M. Childs, E. Farhi, and J. Preskill, *Phys. Rev. A* **65**, 012322 (2001).
- [29] M. S. Sarandy and D. A. Lidar, *Phys. Rev. Lett.* **95**, 250503 (2005).
- [30] J. Aberg, D. Kult, and E. Sjöqvist, *Phys. Rev. A* **72**, 042317 (2005).
- [31] J. Roland and N. J. Cerf, *Phys. Rev. A* **71**, 032330 (2005).
- [32] D. Aharonov and M. Ben-Or, in *Proceedings of 37th Conference on Foundations of Computer Science (FOCS)* (IEEE Comput. Soc. Press, Los Alamitos, CA, 1996) p. 46.
- [33] T. Albash, V. Martin-Mayor, and I. Hen, (2017), 10.1103/PhysRevLett.119.110502, arXiv:1703.03871.
- [34] E. Farhi, J. Goldstone, and S. Gutmann, "Quantum adiabatic evolution algorithms with different paths," (2002), arXiv:quant-ph/0208135.
- [35] A. Perdomo-Ortiz, S. E. Venegas-Andraca, and A. Aspuru-Guzik, *Quantum Information Processing* **10**, 33 (2011).
- [36] E. Crosson, E. Farhi, C. Y.-Y. Lin, H.-H. Lin, and P. Shor, arXiv preprint arXiv:1401.7320 (2014).
- [37] E. Farhi, D. Gosset, I. Hen, A. W. Sandvik, P. Shor, A. P. Young, and F. Zamponi, *Phys. Rev. A* **86**, 052334 (2012), (arXiv:1208.3757).
- [38] B. Seoane and H. Nishimori, *J. Phys. A* **45**, 435301 (2012).
- [39] Y. Seki and H. Nishimori, *J. Phys. A* **48**, 335301 (2015).
- [40] L. Zeng, J. Zhang, and M. Sarovar, *Journal of Physics A: Mathematical and Theoretical* **49**, 165305 (2016).
- [41] L. Hormozi, E. W. Brown, G. Carleo, and M. Troyer, arXiv:1609.06558 (2016).
- [42] N. G. Dickson and M. H. Amin, (2011), 10.1103/PhysRevA.85.032303, arXiv:1108.3303.
- [43] Y. Susa, Y. Yamashiro, M. Yamamoto, and H. Nishimori, (2018), 10.7566/JPSJ.87.023002, arXiv:1801.02005.
- [44] Y. Susa, Y. Yamashiro, M. Yamamoto, I. Hen, D. A. Lidar, and H. Nishimori, "Quantum annealing of the p -spin model under inhomogeneous transverse field driving," (2018), arXiv:1808.01582.
- [45] M. Ohkuwa, H. Nishimori, and D. A. Lidar, (2018), 10.1103/PhysRevA.98.022314, arXiv:1806.02542.
- [46] A. D. King, J. Carrasquilla, I. Ozfidan, J. Raymond, E. Andriyash, A. Berkley, M. Reis, T. M. Lanting, R. Harris, G. Poulin-Lamarre, A. Y. Smirnov, C. Rich, F. Altomare, P. Bunyk, J. Whittaker, L. Swenson, E. Hoskinson, Y. Sato, M. Volkmann, E. Ladizinsky, M. Johnson, J. Hilton, and M. H. Amin, (2018),

10.1038/s41586-018-0410-x, arXiv:1803.02047.

- [47] J. Johansson, P. Nation, and F. Nori, *Computer Physics Communications* **184**, 1234 (2013).
 [48] J. Johansson, P. Nation, and F. Nori, *Computer Physics Communications* **183**, 1760 (2012).

- [49] S. Bravyi, J. M. Gambetta, A. Mezzacapo, and K. Temme, "Tapering off qubits to simulate fermionic hamiltonians," (2017), arXiv:1701.08213.
 [50] L. Veis and J. Pittner, *The Journal of Chemical Physics* **140**, 214111 (2014).

Appendix A: Molecules used in the numerical experiments

In the main text, we considered H_2 , P_4 , and LiH . The geometries of these molecules are shown in Fig. 7. The nuclei separation distance for H_2 and LiH is 1 Å. For P_4 , the intermolecular separation distance for each hydrogen molecule is 2 Å, and d represents the separation distance of the two hydrogen molecules. We investigated d between 0.4 Å and 4 Å.

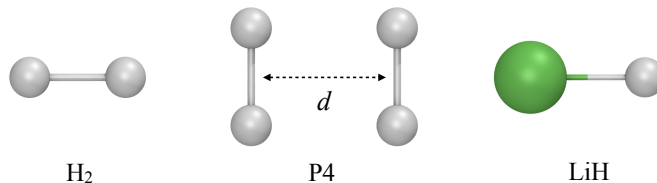


FIG. 7. The geometry of H_2 , P_4 , and LiH .

Appendix B: VanQver algorithm

Algorithm 1 *VanQver*

- Step 1.** Determine the time profiles $A(t)$, $B(t)$, and $C(t)$ and an initial and navigator Hamiltonians $H_{\text{ini}}(\boldsymbol{\eta})$ and $H_{\text{nav}}(\boldsymbol{\theta})$ to define the dependent Hamiltonian $H_{(\boldsymbol{\eta}, \boldsymbol{\theta})}(t) = A(t)H_{\text{ini}}(\boldsymbol{\eta}) + B(t)H_{\text{fin}} + C(t)H_{\text{nav}}(\boldsymbol{\theta})$.
Step 2. Set an annealing time T and the initial and navigator variational parameters $\boldsymbol{\eta} = \boldsymbol{\eta}_0$ and $\boldsymbol{\theta} = \boldsymbol{\theta}_0$ for a quantum device. Set the tolerance for termination ϵ_{tol} for a classical optimizer.
Step 3. Run the AQC algorithm on a quantum device with the time-dependent Hamiltonian $H_{(\boldsymbol{\eta}, \boldsymbol{\theta})}(t)$ to generate a quantum state $|\psi_{(\boldsymbol{\eta}, \boldsymbol{\theta})}(T)\rangle = \mathcal{T} \exp(-i \int_0^T H_{(\boldsymbol{\eta}, \boldsymbol{\theta})}(t) dt) |\psi(0)\rangle$.
Step 4. Estimate the expectation value of the final Hamiltonian $E = \langle \psi_{(\boldsymbol{\eta}, \boldsymbol{\theta})}(T) | H_{\text{fin}} | \psi_{(\boldsymbol{\eta}, \boldsymbol{\theta})}(T) \rangle$.
Step 5. Send $(E, \boldsymbol{\eta}, \boldsymbol{\theta})$ to a classical computer and use a classical optimizer to generate a new set of values for variational parameters $(\tilde{\boldsymbol{\eta}}, \tilde{\boldsymbol{\theta}})$.
Step 6. Send $(\tilde{\boldsymbol{\eta}}, \tilde{\boldsymbol{\theta}})$ to the quantum hardware.
Step 7. Repeat **Step 3** through **Step 6** until the energy E converges with ϵ_{tol} .
Step 8. Output the energy E .
-

Detailed steps of VanQver are shown in Algorithm 1. In the case of our numerical simulations, in **Step 1** we chose $A(t) = 1 - (\frac{t}{T})^2$, $B(t) = (\frac{t}{T})^2$, and $C(t) = \frac{t}{T} (1 - \frac{t}{T})$ (see Fig. 8).

In **Step 4** of Algorithm 1, there is a slight difference between combinatorial optimization problems and quantum simulations. In the case of combinatorial optimization problems, H_{fin} is a classical Hamiltonian and the final state is a classical state. Therefore, measuring all the qubits in the computational basis will give an expectation value of H_{fin} . In the case of quantum simulations, terms in H_{fin} do not commute with each other and the final state will be an entangled state. Therefore, the number of required measurements will increase significantly. Let $H_{\text{fin}} = \sum_k h_k \sigma_1^k \otimes \sigma_2^k \otimes \dots \otimes \sigma_N^k$, where $\sigma_i^k \in [\sigma^x, \sigma^y, \sigma^z, \mathbb{I}]$. We group the terms into mutually commuting contributions, so the terms of each group can be measured simultaneously. If the required measurement for grouped terms is not in the computational basis, a change of basis is needed which can be implemented using single-qubit rotations so that all the terms are functions of only σ^z or \mathbb{I} . For instance, $\mathbb{I} \otimes \mathbb{I} \otimes \sigma^x \otimes \sigma^x$ and $\mathbb{I} \otimes \sigma^x \otimes \sigma^x \otimes \mathbb{I}$ commute with each other. Therefore, they are included in the same group for the purpose of measurement. In order to perform a measurement in the computational basis,

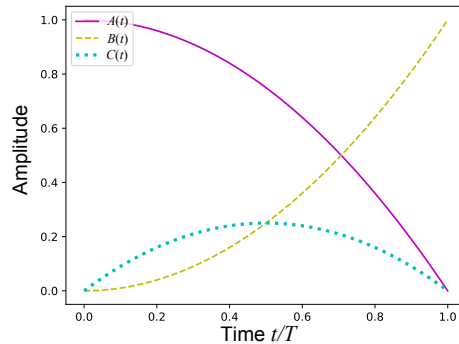


FIG. 8. Amplitude functions $A(t)$, $B(t)$, and $C(t)$ used in our numerical calculations.

we need to rotate the second, third, and fourth qubits from the x direction to the z direction. This idea was first suggested by [10] in the context of the gate model VQE.

The algorithm, in addition to being a hybrid quantum–classical algorithm, is also a hybrid of adiabatic evolution and gate model quantum computation. Instead of using a parametric circuit of quantum gates, the state preparation step is implemented using a parametric adiabatic evolution. Once the state preparation has been performed, we use an expectation estimation approach borrowed from gate model quantum computing to obtain an estimate of the energy of the current state.

Appendix C: Numerical results for H_2 and LiH

In the main text, we show the results for P4. The results for H_2 and LiH are shown in Fig. 9, in which the

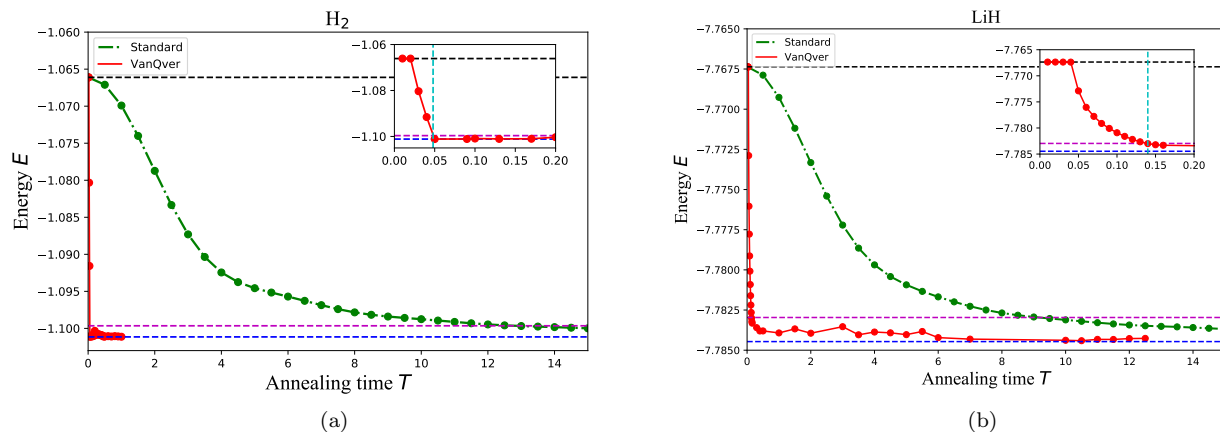


FIG. 9. The energy and annealing time for H_2 and LiH. The red points represent the results obtained using VanQver, the green points represent the results obtained using standard AQC with $H_{\text{ini}} = H_{\text{MP}}$, and the dotted lines in blue and magenta represent the exact and chemical accuracy energies, respectively. The dotted line in light blue in the insets represents T_{CA}^{VanQver} .

energy $E = \langle H_{\text{fin}} \rangle$ is a function of the annealing time T for H_2 (Fig. 9(a)) and LiH (Fig. 9(b)). In standard AQC, the annealing time to chemical accuracy is $T_{CA}^{\text{Standard}} = 13$ for H_2 and $T_{CA}^{\text{Standard}} = 9.5$ for LiH. This shows that the difficulty of the computation depends not only on the number of qubits used to represent the molecule but also the distance between nuclei. In VanQver, $T_{CA}^{\text{VanQver}} = 0.048$ for H_2 and $T_{CA}^{\text{VanQver}} = 0.14$ for LiH.

Appendix D: Classical optimizer dependence

Although the main claim of this work is that VanQver allows us to reach chemical accuracy in energy estimation in a shorter annealing time than standard AQC, it nevertheless relies on classical optimizers to converge to the solution. These optimizers determined what level of accuracy was achievable in our experiments and how many iterations were necessary to reach it. In our code, we used the library QuTip to simulate AQC and the BFGS solver from the SciPy library function `scipy.minimize` as a classical optimizer.

For a given annealing time T , the obtained energy E depends on the tolerance for termination ϵ_{tol} set for the classical optimizer. We compare the quality of the solution obtained after short annealing times $T = 0.03, 0.04$, and 0.05 with different tolerances $\epsilon_{tol} = 0.001, 0.005$, and 0.0001 in Fig. 10(a). The figure shows that the tolerance constraint ϵ_{tol} had a significant impact on the final energy found. However, setting this parameter to a smaller value incurred an increased computational cost. Fig. 10(b) shows that the computational cost induced by decreasing ϵ_{tol} became more important with smaller values of ϵ_{tol} , as reflected by the number of iterations required. For a sufficiently small ϵ_{tol} , further increases in accuracy would impose a severe computational overhead.

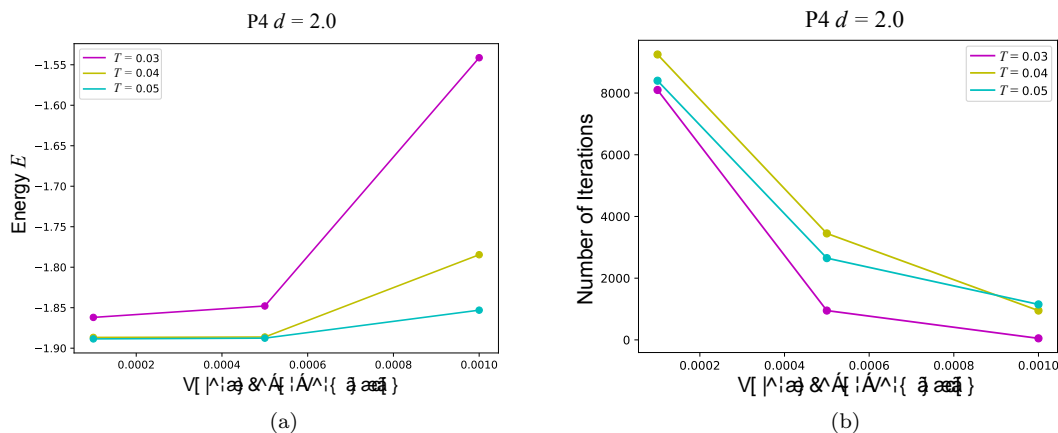


FIG. 10. The tolerance for the termination dependence of the final expectation value of E for $T = 0.03, 0.04$, and 0.05 , for P4 with $d = 2.0$.

Fig. 11 plots the energy of the system against the number of iterations, in this case for P4 with $d = 0.8$ and an annealing time of $T = 0.09$. The classical optimizer spent the first 1000 iterations exploring parameters, returning an energy value close to the HF energy, before dropping quickly to a lower-energy state within chemical accuracy after about 1650 iterations, showing that it may take a long time for the optimizer to find the correct direction to update variational parameters in the parameter space. Convergence can be improved by conducting a sampling of the energy surface in parallel in order to quickly identify a promising direction for the search, before further iteration.

Fig. 12 shows the number of iterations as a function of annealing time T for P4 with $d = 0.8$. When the annealing time was too short, the optimizer converged quickly without improving the result, and the obtained energy was the HF energy. Increasing the annealing time, we observed dramatic improvements in the quality of the solution over a small window of T , between $T = 0.05$ and 0.09 , as shown in Fig. 2. This coincides with the peak number of iterations in Fig. 12, showing that this improvement can be attained at the cost of additional iterations; we noticed that chemical accuracy was reached for $T_{CA}^{\text{VanQver}} = 0.088$. As we further increased the annealing time $T \geq T_{CA}^{\text{VanQver}}$, we noticed that chemical accuracy was always met and that the number of iterations required to converge tended to decrease.

In order to attain a low-energy state of H_{fin} , VanQver relies on H_{nav} to change the annealing path. We can see that tuning the annealing path had a significant impact for shortening annealing times; whereas traditional AQC remained close to the HF energy (see Fig. 2), H_{nav} allowed us to attain chemical accuracy after a large number of iterations. Increasing the annealing time resulted in broadening the range of annealing paths to obtain the accurate energy, allowing the optimizer to attain convergence in fewer iterations.

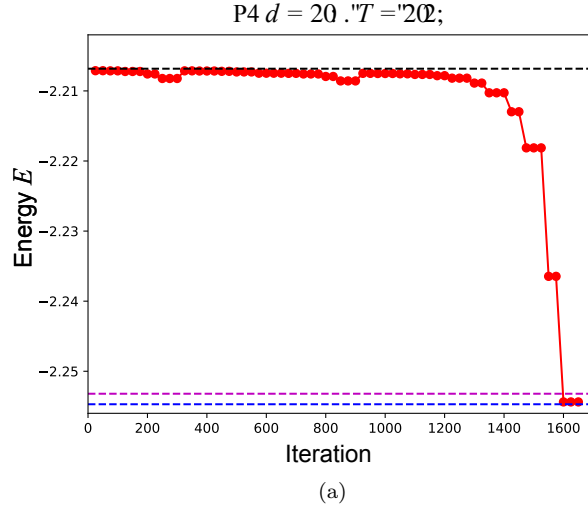


FIG. 11. The energy E vs. the number of optimizer iterations for P4 at $d=0.8$ and $T = 0.09$, with $\epsilon_{\text{tol}}=0.001$. It is noteworthy that our implementation, based on a restarting strategy used to circumvent a memory issue in QuTip, may have increased the number of iterations required to reach chemical accuracy. The kinks around 300 and 700 iterations represent where the restarting occurred. The graph spans the entire computational effort.

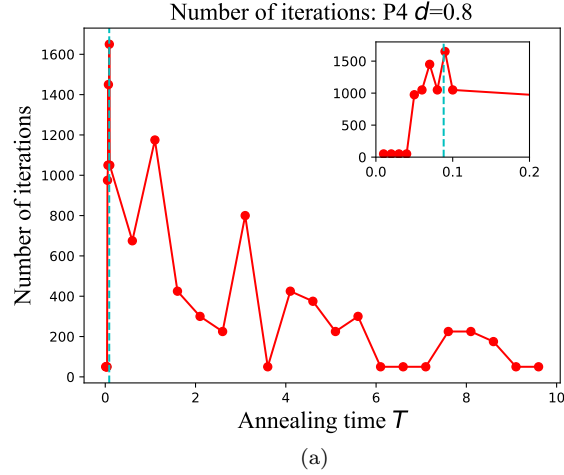


FIG. 12. The number of iterations before convergence vs. annealing time for P4 at $d = 0.8$. The tolerance for termination was set to $\epsilon_{\text{tol}}=0.001$. The time to chemical accuracy was $T_{CA}^{\text{VanQver}} = 0.088239751$, shown using a dotted line in cyan.

Appendix E: The Hartree–Fock Hamiltonian

From a fermionic Hamiltonian perspective, an initial Hamiltonian may consist of one-electron terms

$$H_{\text{ini}}^{\text{ferm}} = \sum_p h_{pq} a_p^\dagger a_q, \quad (\text{E1})$$

which includes the HF Hamiltonian. The form of the initial qubit Hamiltonian used in the numerical experiment appears under JW transformation when the fermionic Hamiltonian is diagonal in a basis of canonical Hartree-Fock orbitals. In our numerical simulations, we employed the canonical RHF Hamiltonian used in [50]. Equation (E2) is

the HF Hamiltonian for H_2 with a nuclei separation distance of 1 \AA :

$$H_{\text{MP}} = \sum_{i=1}^4 h_i \sigma_i^z + h_I \mathbb{I}. \quad (\text{E2})$$

The coefficients are $h_1, h_2 = 0.2422208402$, $h_3, h_4 = -0.2287509695$, and $h_I = 0.50223746961$. The first and second qubits represent occupied spin-orbitals and the third and fourth qubits represent virtual spin-orbitals. Therefore, the signs of the coefficients were appropriately chosen for our purpose. Note that the eigenvalue of H_{MP} does not provide the HF energy.